Catalyzed Decomposition of Urea. Molecular Dynamics Simulations of the Binding of Urea to Urease†

Guillermina Estiu and Kenneth M. Merz, Jr.*

Department of Chemistry, The Pennsylvania State University, 104 Chemistry Building, University Park, Pennsylvania 16802

Received October 5, 2005; Revised Manuscript Received January 13, 2006

ABSTRACT: We present the results of molecular dynamics simulations on the urea/urease system. The starting structure was prepared from the 2.0 Å crystal structure of Benini et al. [(1999) *Struct. Folding Des. 7,* 205−216] of DAP-inhibited urease (PDB code 3UBP), and the trimeric structure (2479 residues) resulted in 180K atoms after solvation by water. The force field parameters were derived using the bonded model approach described by Hoops et al. [(1991) *J. Am. Chem. Soc. 113,* 8262−8270]. Three different systems were analyzed, each one modeling a different protonation pattern for the His320 and His219 residues. In each case, the three monomers of urease have been analyzed separately. The time-averaged structures observed in the three monomers suggest that urease could follow two different competitive mechanisms. A "protein-assisted proton transfer" mechanism points to Asp221 as crucial for catalysis. An "Asp-mediated proton transfer" involves the transfer of a proton from the bridging OH to an NH_2 moiety of urea, assisted by Asp360 in the active site. The impact of the simulation results on our understanding of urease catalysis is discussed in detail.

The reliable prediction of the mechanism involved in the selectivity and efficiency of enzyme-catalyzed reactions continues to challenge both experimental and computational researchers (*3*−*9*). Mutagenic and biochemical procedures, as well as a variety of computational methodologies, have been applied with the goal of understanding the enzymatic effect on reactivity, and several working hypotheses have been proposed. Among them, there is general agreement of the role played by the reduction of the free energy of activation (*3*), but the origin of the free energy lowering, which involves noncovalent and covalent effects, is the subject of ongoing debate (*10*). Noncovalent factors involve transition state electrostatic stabilization (*11*), ground state destabilization and desolvation (*12*), reduction of reorganization energy by binding in near attack conformations (*13*), and entropy trapping (*14*), as well as several other related effects. Covalent and noncovalent effects are not exclusive, and rate enhancement can come from both effects, as well as from others. Covalent factors are dominant, whenever present (*15*). They usually occur in metalloenzymes, where the metal centers covalently bind the substrate, stabilizing the transition state complex and leading to highly proficient catalysts (*10*, *16*). This is the case of the metalloenzyme urease, whose proficiency is presently a matter of extensive discussion, as values of 10^{17} and 10^{32} have been determined by experimental and theoretical means (*17*, *18*).

Urea amidohydrolase (urease) is a nickel-containing enzyme that catalyzes the hydrolysis of urea to produce ammonia and carbon dioxide in the last step of nitrogen mineralization (*1*, *19*−*25*). The mechanism of the catalyzed reaction continues to be of interest, and there is still no agreement on whether the reaction involves a carbamic acid intermediate or a cyanate intermediate or if it proceeds via direct decomposition (*1*, *24*, *26*−*30*). It is well-known that the uncatalyzed reaction proceeds through an elimination pathway, and a cyanate intermediate has been identified in this case (*17*, *31*−*34*). The increase in pH arising from this reaction causes a broad range of deleterious effects. For example, urease is a virulence factor in human and animal pathogens: it participates in the development of kidney stones, pyelonephritis, peptic ulcers, and other disease states (*1*, *19*−*22*, *24*). In particular, *Helicobacter pylori*, a Gram-negative microaerophilic bacterium first isolated in the stomach of patients with gastritis and peptic ulcers, produces a large amount of urease which is believed to play an essential role in facilitating bacterial survival (*35*−*37*). *H. pylori* infection has also been linked to several gastroduodenal diseases including cancers. The presence of urease activity in soils is exploited in fertilization, although excessive levels of urease in soil can degrade urea applied as a fertilizer too rapidly and result in phytopathic effects and loss of volatilized ammonia (*26*). The enzyme urease also catalyzes the hydrolysis of hydroxyurea to hydroxylamine, enhancing the formation of iron nitrosyl hemoglobin which is used in the treatment of sickle cell anemia (*38*). In addition to the importance of urease to agriculture and medicine, the structure and catalytic mechanism of this enzyme are of interest because of its large enhancement (at least 10^{14}-fold) of the rate of urea hydrolysis (*17*) and the presence of nickel in the active site, which is unique among hydrolytic enzymes.

Structural studies of the enzymes from *Klebsiella aerogenes*, *Bacillus pasteurii*, and *H. pylori* have revealed a

† This work was supported by NIH Grant GM066859. We also thank the NCSA and PSC for supercomputing support.

* To whom correspondence should be addressed at the Department of Chemistry, Quantum Theory Project, University of Florida, 2328 New Physics Building, P.O. Box 118435, Gainesville, FL 32611-8435. Phone: 352-392-6973. Fax: 352-392-8722. E-mail: merz@qtp.ufl.edu.

10.1021/bi052020p CCC: $33.50
Published on Web 03/18/2006

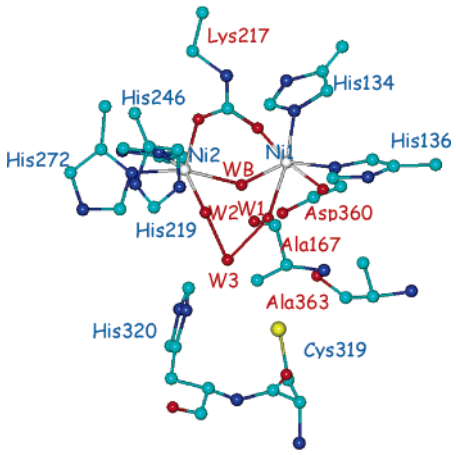

FIGURE 1: Active site of the dinickel urease enzyme from *K. aerogenes* (PDB code 1FWJ) determined by X-ray crystallography. In all figures O is in red, N is in blue, C is in blue-green, S is in yellow, and Ni is in gray.

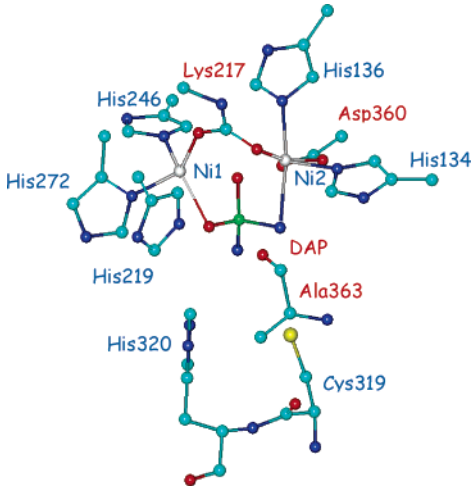

FIGURE 2: Active site of the DAP-inhibited urease enzyme from *B. pasteurii* (PDB code 3UBP) determined by X-ray crystallography. In all figures O is in red, N is in blue, C is in blue-green, S is in yellow, P is in green, and Ni is in gray.

dinuclear Ni active site with a modified amino acid side chain (a carbamylated lysine residue) that bridges the metal ions, along with a deprotonated water molecule (WB, Figure 1) (*1*, *20*−*22*, *24*). These structural features are frequently found in dinuclear metallohydrolases, where bridging aspartate residues are usually involved (*39*). Remarkably, the binuclear center of urease is identical to those of dihydroorotase and phosphotriestearase, where Zn, Cd, or Co ions replace Ni (*40*). The bridging water molecule is thought to be deprotonated on the basis of the pK_a value of a water molecule ligand in hexaaquo-Ni^{2+} (10.6) and the optimum pH (8) for catalytic activity (*1*). The bridging water molecule is thought to be catalytically relevant and is partially responsible for the pH dependence of the catalytic activity, which decreases as the pH decreases (*1*, *24*). The presence of two metal ion bridging groups accounts for the observation of weak antiferromagnetic coupling (*24*).

The microbial ureases of *K. aerogenes* and *B. pasteurii* are essentially identical in terms of backbone structure (*1*, *24*). The three α subunits, constituting the core of an $(\alpha\beta\gamma)_3$ trimer of trimers, consist of an $\alpha\beta$ barrel domain and a β-type domain. The β subunits, located on the surface of the trimer of trimers, feature a predominantly β structure. Finally, the γ subunits consist of $\alpha\beta$ domains located on top of each pair of α subunits (*24*). All residues in the protein are well ordered except for residues 308−337 on the α chain, which forms a mobile flap that covers the active site. Open and closed conformations of the mobile flap have been experimentally observed in urease structures from different species (*1*, *19*−*27*, *41*−*45*). The closed conformation has been reported for the *K. aerogenes* urease structure (KAU, PDB code 1FWJ) (*24*), while the open conformation has been observed in the X-ray structure of *B. pasteurii* urease (BPU, PDB code 2UBP) (*1*). For the β-mercaptoethanol (BME; PDB code 1UBP) (*20*) and acetohydroxamic acid (AHA; PDB code 4UBP) (*21*) inhibited ureases, the mobile flap is found in the open conformation. However, for the diaminophosphate (DAP) inhibited BPU (PDB code 3BPU), the flap is found in the closed conformation (*1*, *42*). For simplicity, the atom numbering of 1FWJ will be used throughout this paper.

The dinuclear active sites of the three monomers are 70 Å apart and behave independently (*20*, *24*). In the urease active site, one of the Ni centers [Ni(1)] has a distorted pyramidal geometry, defined by two imidazole ligands from two His residues and a water molecule. The other Ni atom [Ni(2)] is in an octahedral environment, which is formed by the coordination of two histidine imidazoles, an aspartate, and a water molecule (see Figure 1) (*1*, *20*, *24*). A third water molecule interacts with the bridging OH and also with the other water molecules, producing a tetrahedral-shaped electron density map (*1*). These water molecules may be either partially or completely displaced by urea coordination (*46*).

Coordination Mode of Urea and Inhibitors. Several structures of inhibitors complexed with BPU are available, all of them indicating that the terminal water molecules and the bridging hydroxide are quite labile (*1*, *19*−*22*). Among them, the structures of BPU, complexed by DAP (*1*) and by boric acid (*22*), have strongly influenced the prediction of the coordination mode of urea. $B(OH)_3$ is considered a substrate analogue, from which molecular details of substrate binding can be inferred (*22*). DAP, on the other hand, has been proposed to be a transition state analogue, in which the bridging OH participates in the bonding (*1*).

DAP binds the bimetallic center using three of the four potentially coordinating atoms: one DAP oxygen atom replaces the Ni-bridging hydroxide, one DAP oxygen and one nitrogen atom bind to Ni(1) and Ni(2), respectively, while the second nitrogen atom points away, toward the opening of the active site cavity. This coordination mode holds the flap in a closed conformation, allowing hydrogen bond interactions with key residues: the Ni(2)-bound DAP nitrogen has a hydrogen bond with the carbonyl oxygen atoms of Ala167 and Ala363 while the distal DAP donates a bifurcated hydrogen bond to the carbonyl oxygen atom of Ala363 and to His320 (see Figure 2) (*1*).

Boric acid is symmetrically placed between the Ni atoms, without perturbing the bridging OH, leaving the flap in an open conformation, as found in the native enzyme. Two inhibitor oxygen atoms are bound to the Ni ions, while the third oxygen atom points toward the active site opening, away from the Ni atoms. The Ni(2)-bound inhibitor oxygen atom forms a hydrogen bond with the backbone oxygen of Ala167, while the uncoordinated OH group of the inhibitor

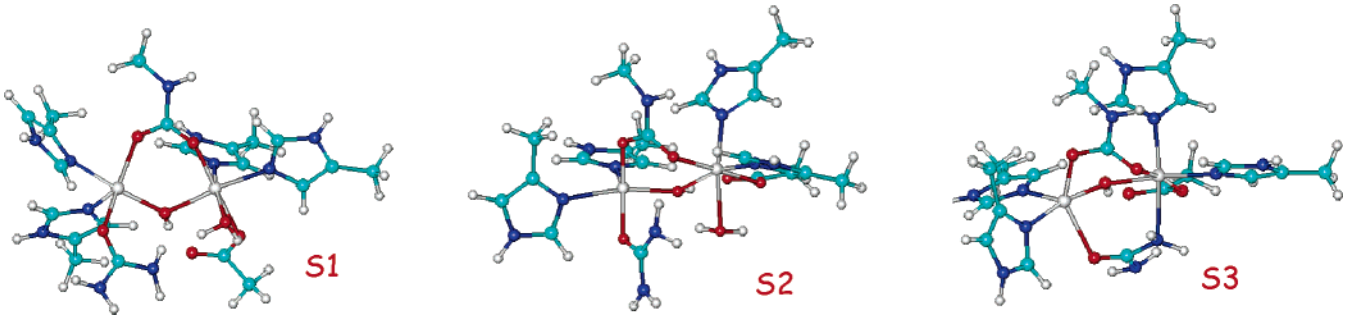

FIGURE 3: B3LYP/LAPCV* optimized structures of the urea-bound complexes. S1 and S2 represent monodentate coordination modes, stabilized by hydrogen bond interactions between the inter-Ni OH and the amide NH_2 end (S1) or a water molecule that is kept in the active site (S2). S3 is a model of the bidentate coordination mode.

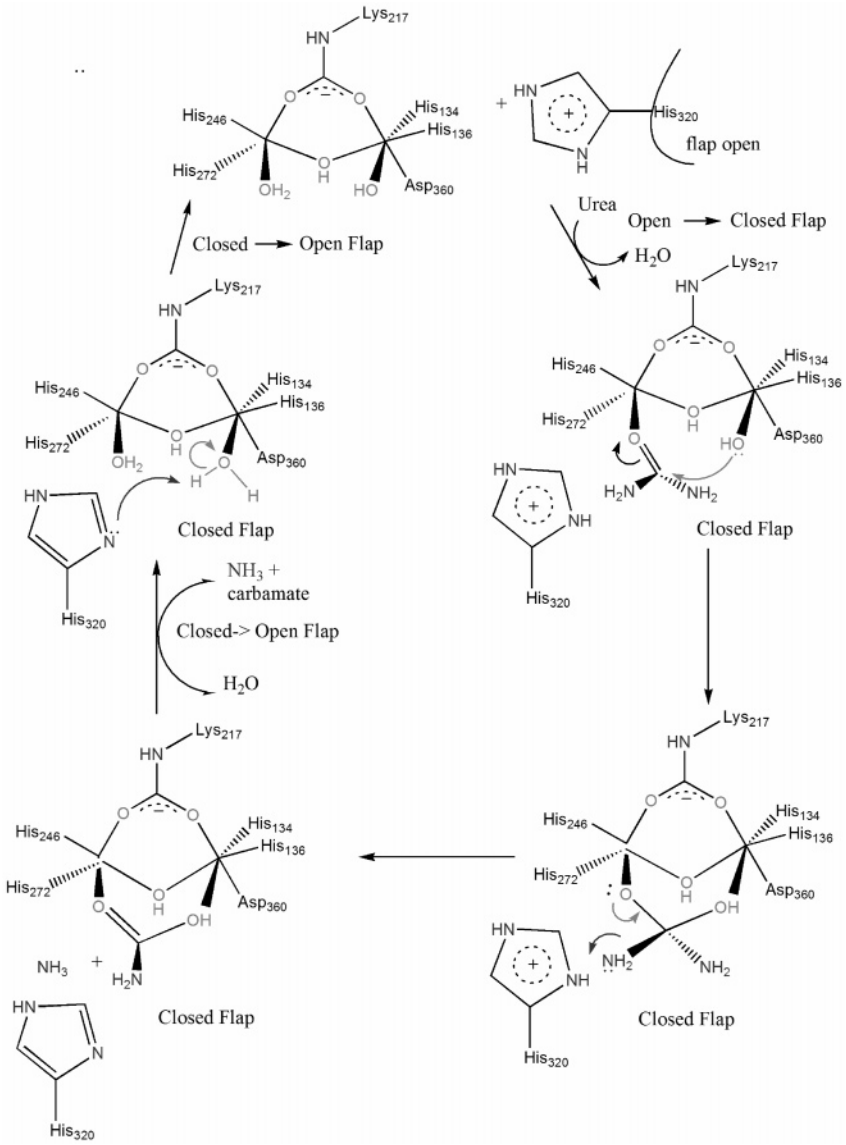

FIGURE 4: Structurally detailed mechanism for urease catalysis adapted from Karplus and Hausinger (*24*). The reaction proceeds through a tetrahedral intermediate that gives carbamic acid after NH_3 release. It is based on the assumptions that a water molecule is retained after urea coordination and that His320 is protonated.

is hydrogen bonded to a water molecule involved in a hydrogen-bonding network with an additional solvent molecule and the carbonyl oxygen of Ala363 (*22*).

Urea is assumed to bind its carbonyl oxygen atom to Ni(1), displacing either two or three water molecules from the active site, to give the geometries shown in Figure 3(*46*). When three water molecules are removed, one of the NH_2 groups of the urea molecule also binds Ni(2) (see S3, Figure 3). Flap closure has been suggested to help in stabilizing this geometry, allowing key residues, for example, His320 and Ala363, to approach the Ni cluster (*1*). However, a monodentate coordination mode, such as S1 and S2 shown in Figure 3, can also be stabilized by hydrogen bond interactions with residues of the flexible loop (*24*). Bidentate coordination

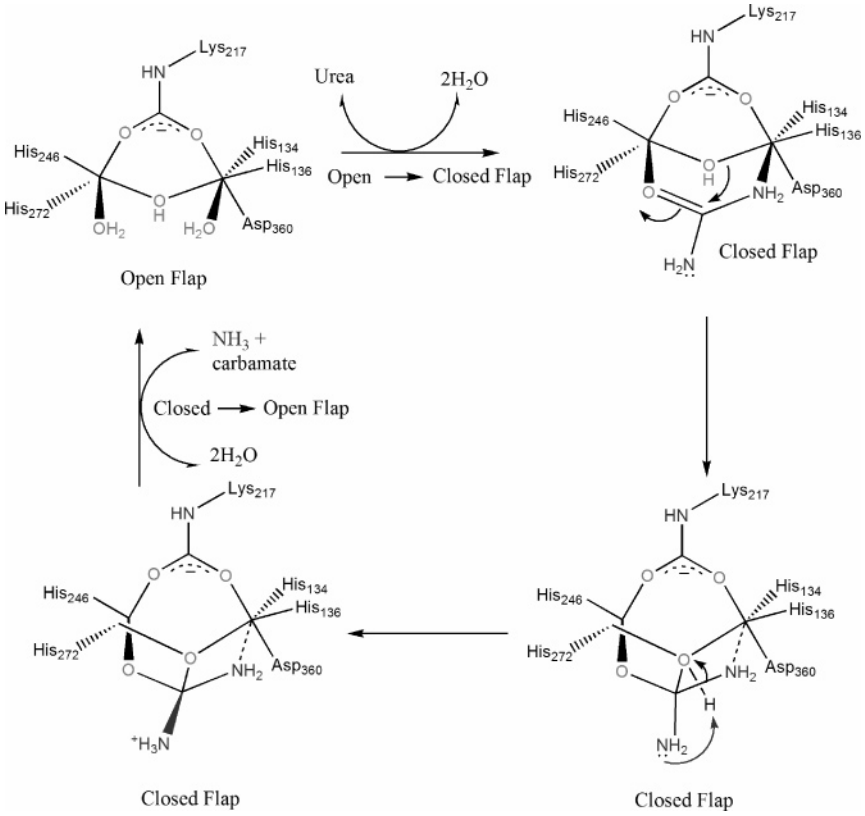

FIGURE 5: Structurally detailed mechanism for urease catalysis adapted from the one proposed by Benini et al. (*1*). The reaction proceeds through a tetrahedral intermediate that gives carbamic acid after NH_3 release. The bridging OH acts as a nucleophile toward the carbonyl carbon and also protonates the distal NH_2.

has been supported by the structures of DAP- and $B(OH)_3$-inhibited urease (*1*, *22*), while recent quantum chemical calculations favored a monodentate structure, in which further stabilization is attained by hydrogen bond coordination of one amide hydrogen atom with the bridging Ni OH (*46*).

Proposed Reaction Mechanisms. The reaction mechanism of enzyme-catalyzed urea decomposition has been the subject of debate since the early 1920s (*28*−*30*). Three main reaction pathways have been proposed: the carbamic acid (hydrolytic) mechanism, which involves a carbamic acid (or carbamate) intermediate, a carbon dioxide mechanism, in which the molecule is directly hydrolyzed to carbon dioxide and ammonia, and a cyanic acid (elimination) mechanism, associated with the formation of cyanate intermediates (*28*). From studies of the chemistry and biochemistry of bacterial urease from *K. aerogenes* and *B. pasteurii* a mechanism of catalysis and inhibition of the enzyme at a molecular level has been recently proposed, which can be classified as a carbamic acid mechanism (*1*, *24*).

The mechanism proposed by Karplus for KA (Figure 4) is based on two main assumptions (*24*): (1) Urea coordinates in a monodentate manner, binding the carbonyl oxygen atom to Ni(1) and retaining a water molecule in the Ni(2) site. (2) This water molecule is deprotonated, whereas a residue of the mobile flap (His320) is protonated. Within this scheme, the Ni(2)-bound OH acts as a nucleophile and attacks the carbonyl carbon atom of the urea molecule, which is further polarized by coordination to the Ni center. The reaction proceeds through a tetrahedral intermediate, from which NH_3 is released, assisted by proton transfer from protonated His320. In this mechanism His320 appears to be the most relevant residue for catalysis; however, hydrogen bond interactions with Ala167, Ala363, Cys319, His219, and G277 have been inferred from the X-ray data as well.

In the mechanism proposed by Benini for BPU (see Figure 5), urea binds in a bidentate manner, and the bridging Ni OH plays two roles: it provides the proton that is transferred to the free NH2, facilitating the release of NH3, and provides the nucleophilic oxygen atom that attacks the urea carbonyl carbon atom (*1*). Ala363 and His320 have been proposed to help in positioning urea and in guiding the NH3 molecule out of the active site when the flap opens.

A cyanic acid mechanism has also been proposed on the basis of kinetic studies of biomimetic complexes, which involves elimination of the ammonium ion, assisted by a protein residue, and further hydrolysis of the resulting cyanic acid to give CO_2 and ammonia (see Figure 6) (*31*−*33*). This reaction pathway has been observed in phthalazine-based biomimetics of urease and provides evidence for a mechanism that has long been considered as an alternative pathway for the enzymatic hydrolysis of urea (*47*). Moreover, high-level quantum chemical calculations have demonstrated its feasibility (*34*).

This present research is aimed at determining the coordination mode and reaction mechanism of urease-catalyzed urea decomposition, based on the analysis of multinanosecond MD trajectories of the urea/urease complex. During the course of the simulations, we characterized the role of key residues potentially involved in the decomposition pathway and we compared different protonation states, while enhancing our overall statistics by simultaneously evaluating each of the dinuclear active sites of the trimeric structure. Through the simulations described below we will address mechanistic issues that could impact the design of novel mechanism-

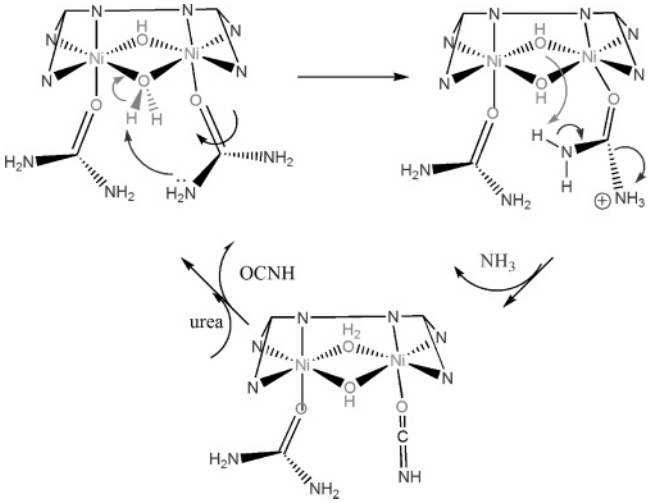

FIGURE 6: Possible mechanism for the urea elimination reaction catalyzed by phthalazine-based urease biomimetics. The second Ni-bound urea molecule can follow a similar mechanistic pathway. The phthalazine ligand has been simplified for clarity.

based inhibitors of the metalloenzyme urease (*48*).

COMPUTATIONAL METHODS

MD Simulations. To analyze the influence of key residues of the protein on the decomposition mechanism, we have chosen to build the urea/urease complex (for which X-ray data are not available) using the closed conformation of the mobile flap. The starting structure was prepared from the 2.0 Å crystal structure of Benini et al. of DAP-inhibited urease (PDB code 3UBP) (*1*), from which the crystallographic waters were stripped. The DAP coordinates were removed and replaced by those corresponding to urea. The coordinates of urea were built from the superposition of the DAP-free 3UBP structure with the optimized model cluster used for the force field parametrization (S3; see Figure 3). From the resulting structure, the trimer was built using locally developed programs.

The ionizable amino acid side chains of the residues close to the active site were assigned their most stable protonation state at pH 8. Special attention was given to His320 and His219, because their protonation state has been debated extensively in the literature (*1*, *21*, *22*, *24*). Accordingly, three different systems were analyzed, each one modeling a different protonation pattern. The first model deprotonates both His320 and His219, and we label this model as UrHisHis (both His320 and His219 are in their neutral deprotonated forms) in the subsequent discussion. The remaining two states involved the uptake of one proton by either His320 or His219, yielding states that we have labeled as UrHip320 (for His320 protonated and His219 deprotonated) or UrHip219 (for His320 deprotonated and His219 protonated).

The urea/urease system was surrounded by a periodic box of TIP3P water molecules, which extended 10 Å out from any protein atoms. This resulted in the protein (2479 residues, 36394 atoms) being solvated by 47618 water molecules. The entire system is composed of 179248 atoms. The LEaP module of AMBER8 (*49*) was used to protonate and to neutralize the system.

To remove bad intra- and intermolecular contacts in the initial geometry, energy minimizations were carried out using

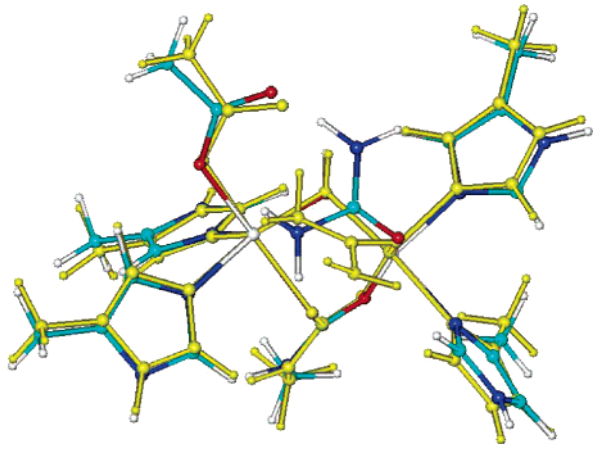

FIGURE 7: QM optimized structures of the urease active site with bidentate coordinated urea. S3 (not colored) is 1.8 kcal/mol lower in energy that S3′ (shown in yellow).

conjugate-gradient minimization (2500 steps for the water molecules followed by 2500 steps for the entire system). MD simulations were carried out using PMEMD included in the AMBER8 suite of programs (*49*). The time step was 1.5 fs, and the SHAKE (*50*) algorithm was used to constrain all bonds involving hydrogen atoms. A nonbond pair list cutoff of 9.0 Å was used, and the nonbonded pair list was updated every 25 time steps. The pressure (1 atm) and the temperature (300 K) of the system were controlled during the MD simulations by Berendsen's method (*51*). Periodic boundary conditions were applied to simulate a continuous system. To include the contributions of long-range electrostatic interactions, the particle-mesh-Ewald (PME) (*52*) method was used. The estimated root mean squared deviations of the PME force errors during the simulations were lower than 10^{-4}. After an equilibration period of 300 ps, a 6 ns trajectory was computed, and the coordinates were saved every 1000 time steps.

Parametrization of the Active Site Nickel Cluster. To derive the corresponding force field parameters which are not present in the standard AMBER database, we used the bonded model approach as described by Hoops et al. (*2*). To ensure compatibility with the AMBER force field, we adopted the protocol outlined by Fox et al. (*53*). This hybrid procedure has been successfully applied to derive the force field of zinc metalloenzymes (*54*). Equilibrium bond lengths and angles involving the Ni(1) and Ni(2) environments were taken from the lowest energy optimized structure that resulted from minimization of cluster models of the urease active site (*46*). The calculations, previously reported by Suarez et al. (*46*), employ the restricted open shell implementation of the B3LYP functional (*55*) (using Jaguar) (*56*) with the 6-31G* basis set (*57*) for nonmetal atoms and the Los Alamos effective core potential (*58*) for the Ni ions. After geometry optimization, the electronic energies of the dinickel complexes were refined by means of single point calculations using the 6-311+G(2d,2p) basis set for nonmetal atoms and a modified version of the LACVP core potential for Ni in which the exponents were decontracted to form a triple-z quality basis set (this basis set is denoted as LACV3P**+) (*59*). For the same model clusters, atomic charges were computed by carrying out natural population analysis (NPA) using the B3LYP/LACV3P**+ density matrices.

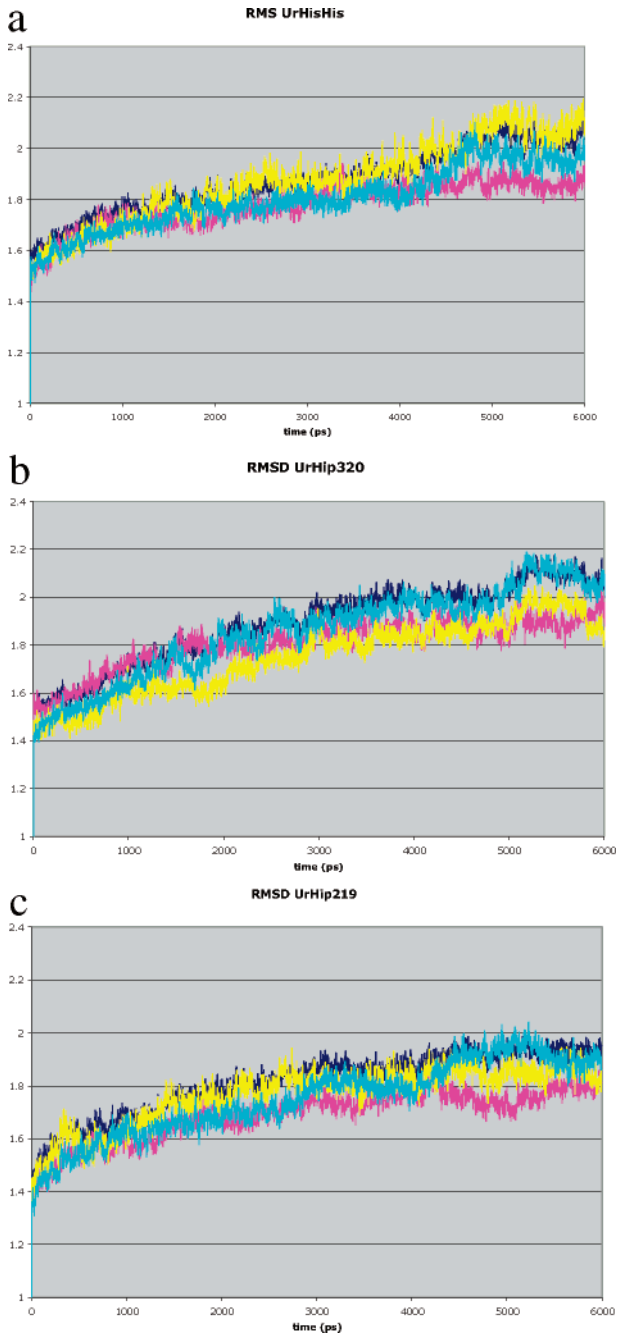

FIGURE 8: Root mean square deviation (in Å) of the 6 ns simulations: (a) UrHisHis, (b) UrHip320, and (c) UrHip219. In the three cases blue corresponds to the trimer structure, pink to the first monomer, yellow to the second monomer, and cyan for the third monomer.

In the model, the Ni ions are bridged by a hydroxide group and the carbamylate group of Lys* and complexed by four methylimidazole ligands and the carboxylate of the Asp side chain (see Figure 1). The parameters were derived for the optimized structure shown in Figure 7 (S3), in which urea is coordinated to both Ni centers. Figure 7 also shows a second possible conformation of bicoordinated urea (S3′, in yellow), which can be generated through rotation around the Ni−O(urea) bond and is only 1.8 kcal/mol less stable than S3 at the same QM level of theory. According to this observation, we built a force field flexible enough to allow for this torsional mode of the urea ligand. The quadratic force constants for the bond (Ni−X) and angle (Ni−X−Y) terms

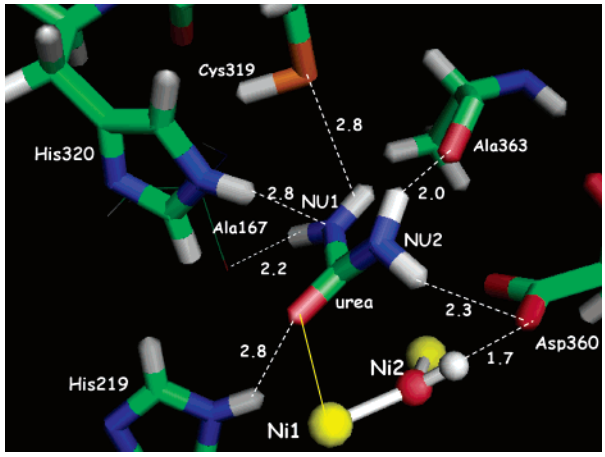

FIGURE 9: Typical snapshot after equilibration of the urea-complexed system showing the H-bond interactions established between the urea ligand and neighbor protein residues. The active site is represented by the Ni atoms (yellow) and the bridging OH.

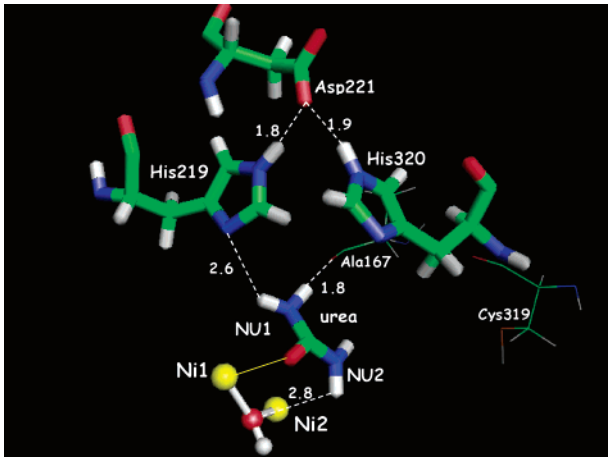

FIGURE 10: Snapshot of UrHisHis showing the most relevant hydrogen bond interactions that are stabilized in the first monomer between the urea ligand and protein residues. Only the Ni atoms (yellow) and the bridging OH are used to represent the active site. The distances are shown in Å, measured at the end of the 6 ns MD run. A stereographic representation is included in the Supporting Information.

were obtained from diagonal elements of the analytically calculated Hessians for small Ni−R and Ni(1)−R−Ni(2) systems projected onto a space of internal coordinates. All of the torsions associated with the Ni−ligand interactions were set to zero as in Hoops et al. (*2*). B3LYP/LACV3P**+ atomic partial charges were derived using the RESP methodology (*60*). In this way, electrostatic interactions between all atoms of the system were treated on an equal basis. The van der Waals parameters for Ni were derived from those reported in Hoops et al., while the atoms in the water molecules and model residues were assigned the standard AMBER atom types. This force field parametrization was initially tested by minimizing in vacuo the geometry of the model complexes (Figure 7), using the PMEMD module included in AMBER8 (*49*). At the molecular mechanics level, the structures differ by 7 kcal/mol. As we further discuss, even though this energy difference is greater than the QM-derived value, fluctuations between both conformations were observed in the MD runs.

All of the parameters used to represent the environment of the active site nickel cluster are included in the Supporting

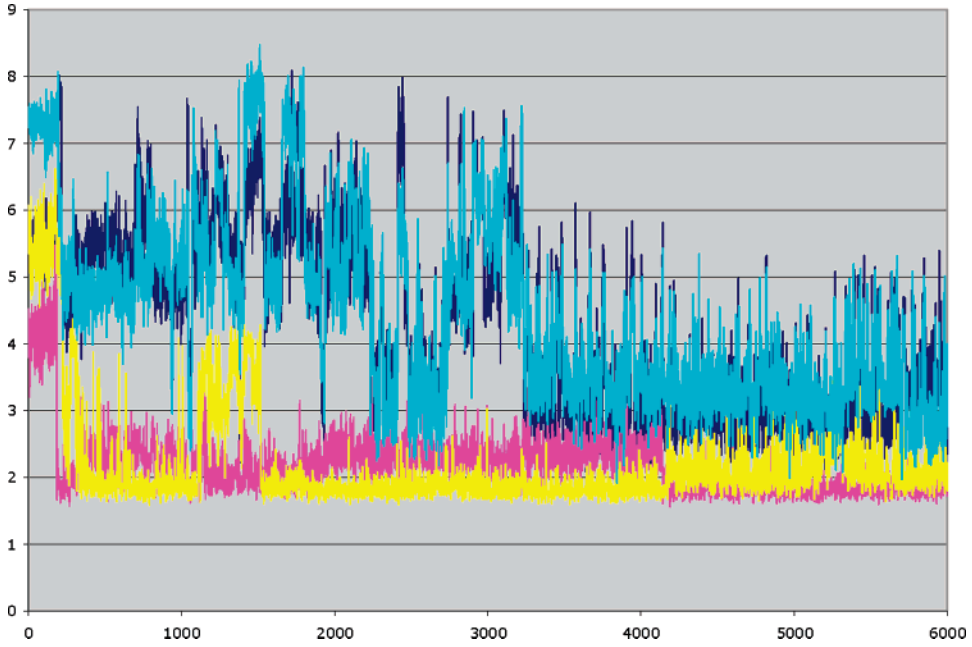

FIGURE 11: Evolution of the distances (in Å) shown in Figure 9 during the 6 ns MD simulation. Key: pink, OD2 at Asp221−HE2 at His219; yellow, OD2 at Asp221−HE2 at His320. The blue and cyan lines represent the separation between ND1 at His219 and the H atoms bonded to the atom labeled NU1.

Information.

RESULTS AND DISCUSSION

Protein Root Mean Square Deviation and Flexibility. The time evolution of the root mean square deviation (RMSD) of the instantaneous structures (Figure 8) was evaluated relative to the optimized structure built from substitution of DAP by urea in the X-ray structure 3UBP. The RMSD value for the entire protein was, on average, 1.88, 1.90, and 1.81 Å for UrHisHis, UrHip320, and UrHip219, respectively. These values, which are similar to those observed in other metalloenzyme simulations (*54*, *61*), do not differ from those evaluated separately for the three monomeric units.

To gain insight into the fluctuations of the enzyme, the RMS flexibility (RMSF) was calculated by comparing the instantaneous protein structure to the average one, yielding values of 1.08, 1.07, and 1.03 Å for UrHisHis, UrHip320, and UrHip219, respectively. We have also calculated the RMSF values for the atoms of the mobile flap of each monomer. They vary between 1.05 and 1.07 Å for the first and second monomer, regardless of the protonation state, while, interestingly, the RMSF increases to 1.2 Å in the third monomer. The increased flexibility of the third monomer will be further analyzed in relation to the participation of the mobile flap in the catalytic mechanism.

Structure of the Active Site. (A) Neutral His Residues, UrHisHis. A typical snapshot of the active site after equilibration is shown in Figure 9 as a visual aid to see the hydrogen bond interactions that can be formed when urea coordination is built from the bidentate QM optimized structure (see Figure 9, S3). Only the residues that establish hydrogen bond interactions with urea are shown. Most of them are residues from the mobile flap, which is believed to play a key role in allowing substrate entrance and in positioning key residues for catalysis (*1*, *21*, *22*, *24*). Asp360 and the bridging OH, belonging to the first coordination shell, are also included. In this structure, one of the NH_2 groups

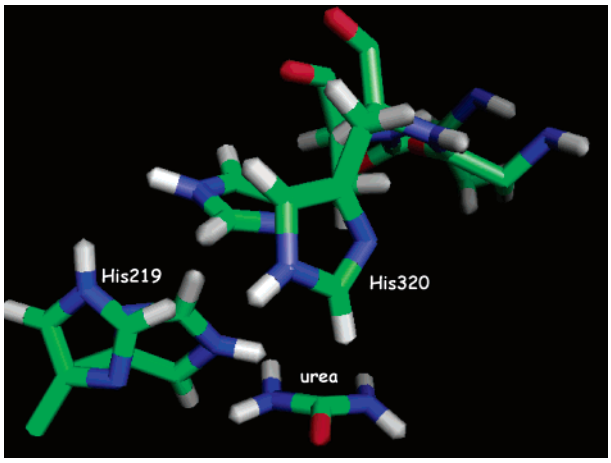

FIGURE 12: Comparison of two snapshots of the first monomer of UrHisHis showing how His320 and His219 can change their orientation relative to urea during MD simulation.

of the urea molecule is stabilized by a hydrogen bond interaction with OD2 at Asp360, which is also at hydrogen-bonding distance with the bridging hydroxide. Within the hydrolytic mechanism (see Figure 5), this coordination mode assists the transfer of the hydroxide proton to an NH_2 group of urea (*1*, *34*), while from the standpoint of the elimination reaction, this coordination represents the onset of a proton transfer from the urea NH_2 to the bridging OH (see Figure 6). The two protons of the other NH_2 moiety are hydrogen bonded to the backbone carbonyl of Ala167 and Ala363, while also accepting hydrogen-bonding interactions with HE2 at His320 and HG at Cys319.

Interactions with these residues have also been described by Karplus et al., after docking the urea molecule into the unligated active site of KAU (PDB code 1FWJ) (*24*), and by Benini et al. (*1*), after a similar analysis of the possible coordination modes of urea in the active site of BPU (PDB code 3UBP). Although involving mainly the same residues, the hydrogen bond coordination pattern shown in Karplus

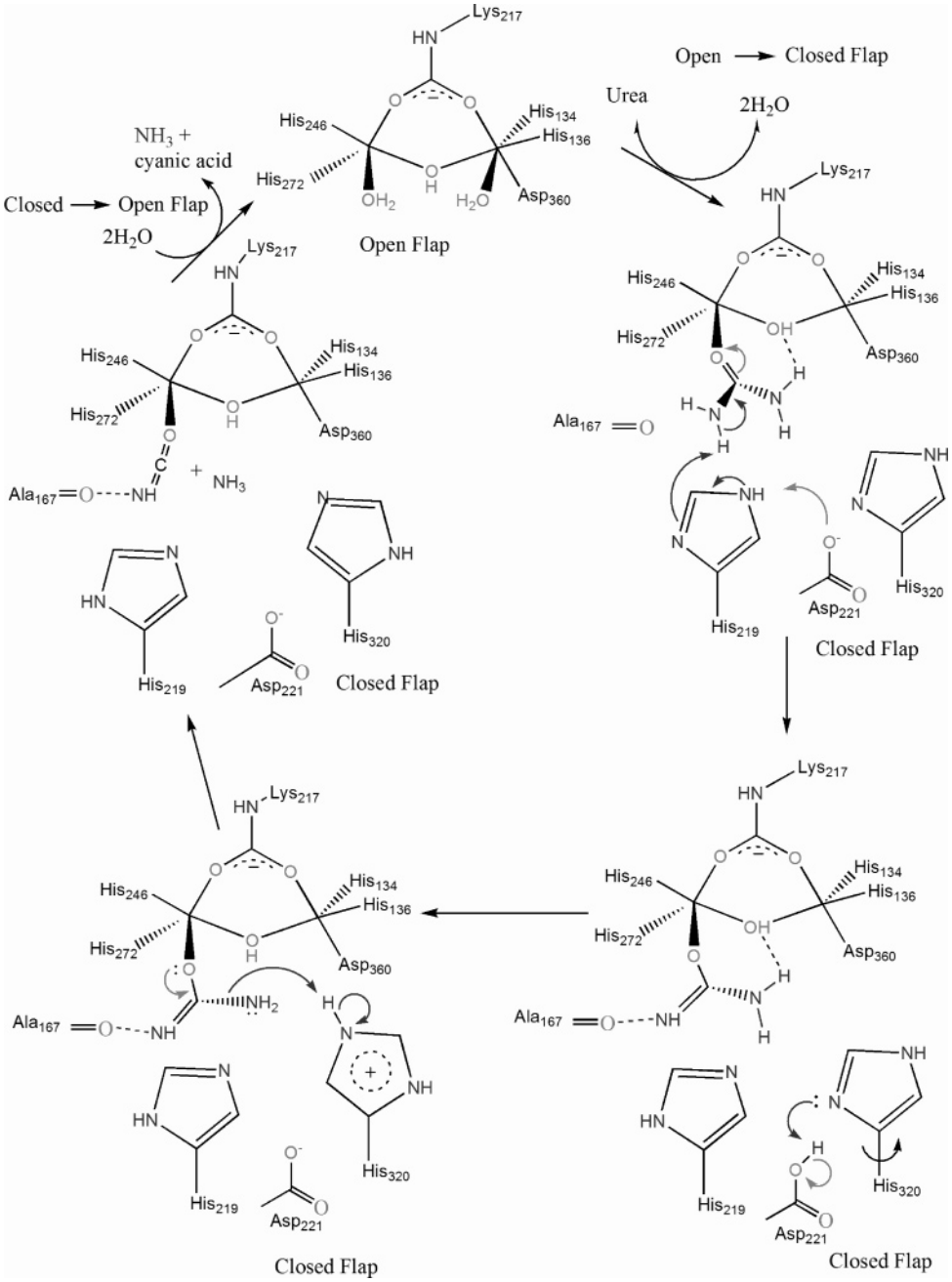

FIGURE 13: Schematic representation of the protein-assisted proton transfer mechanism proposed to occur in the active site of monomer 1.

et al. is different than ours, because the urea molecule is oriented in a way that allows a water molecule to be retained by the second Ni atom of the active site. It is noteworthy that the neutral form of His320 is orientated in a way that allows it to establish a hydrogen bond interaction with a nitrogen atom of urea.

The evolution of the hydrogen-bonding distances during the 6 ns MD simulation shows that the initially established active site hydrogen bond network evolves differently within each of the active sites as the urea molecule accommodates to its possible conformations in the protein environment. The main characteristics of the interaction patterns are shown, for the three monomers, in Figures 9, 13, and 16, respectively (only the most relevant residues are highlighted in each case). We will arbitrarily refer to them as monomer 1, monomer 2, and monomer 3.

In one of the monomers (monomer 1, Figure 10) urea is stabilized by interactions with O at Ala167 and ND1 at His219 from the mobile flap. Thus, an amide nitrogen of urea acts as proton donor in N−H—O and N−H—ND1 interactions, while one of the hydrogen atoms from the other NH_2 group acts as a donor toward the bridging hydroxyl. This last interaction has been found to determine the coordination mode of urea in QM calculations of cluster models of the urease active site (*46*). Although not directly involved in urea coordination, contacts between HE2 at His219 and HE2 at His230 with OD2 at Asp221 are readily identifiable. These residues form a His-Asp-His "triad" that remains stable over the entire MD simulation, with average interresidue distances of 2.15 Å. An analysis of the time evolution of the distances (see Figure 11) shows that, while the His219-Asp221-His230 network is stabilized very soon

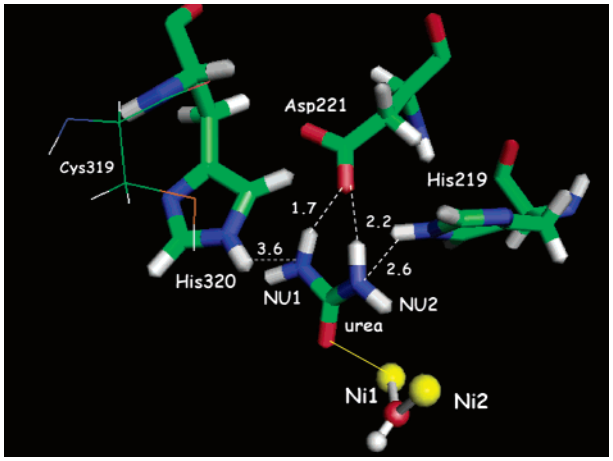

FIGURE 14: Snapshot of UrHisHis showing the most relevant hydrogen bond interactions that are stabilized in the second monomer between the urea ligand and the protein residues. Only the Ni atoms (yellow) and the bridging OH are used to represent the active site. The distances are shown in Å, measured at the end of the 6 ns MD run. A stereographic representation is included in the Supporting Information.

after equilibration, the hydrogen bond interaction between urea and His219 fluctuates until ~3 ns. Prior to this, the hydrogen bond interaction with O at Ala167 alternates between each of the hydrogen atoms of the NH_2 group of urea (see Figure 1 in the Supporting Information), affecting their interaction with His219.

The interaction pattern observed in our simulation leads us to propose a reaction mechanism that has not been described to date. We will refer to this mechanism as a "protein-assisted proton transfer", because the protein residues play a major role in helping to transfer a proton between both NH_2 ends of urea, ultimately catalyzing an elimination pathway (see Figure 6). His219, strongly hydrogen bonded to Asp221, acts as a "histidinate", favoring the deprotonation of urea through a concerted proton transfer from one amide hydrogen to ND1 at His219 and from HE2 at His219 to OD2 at Asp221. Strong hydrogen bonds between His and Asp residues have been previously found to provide "histidinate-like" species, which can be involved in metal center coordination, playing a role in regulating their Lewis acidity (*39*). The next step of the protein-assisted proton transfer is associated with the release of His320 from hydrogen bond coordination with Asp221, after the protonation of the latter. His320 is quite dynamic, as shown in Figure 12, and transfers the HE2 proton to the other NH_2 group of urea. The three residues act in concert in order to play a similar role as a water molecule in the aqueous phase decomposition of urea (*17*). Water-assisted proton transfer mechanisms have previously been found to be energetically favorable for both the aqueous phase decomposition of urea and for the reaction occurring in phthalazine-based biomimetics (*17*, *34*). Within this mechanistic scheme, the resulting NH_3 moiety can be released from urea, assisted by the movement of His320 when the flexible flap opens (*1*). This leaves cyanic acid, which can be further hydrolyzed. A schematic representation of the proposed mechanism is given in Figure 13.

The protein-assisted proton transfer mechanism is further supported by the hydrogen bond network shown in Figure 14, which is observed in the active site of the second monomer of urease. In this case, an even simpler mechanistic scheme can be proposed, because Asp221 can facilitate a proton transfer reaction between the two different NH_2 groups of urea without additional participation of the His residues. This possibility can be inferred from the snapshot obtained after 6 ns of MD simulation, where the hydrogen atoms belonging to different NH_2 moieties of urea are forming long-lived hydrogen bonds with OD2 at Asp221. These interactions are not established before 2.4 ns and are certainly more

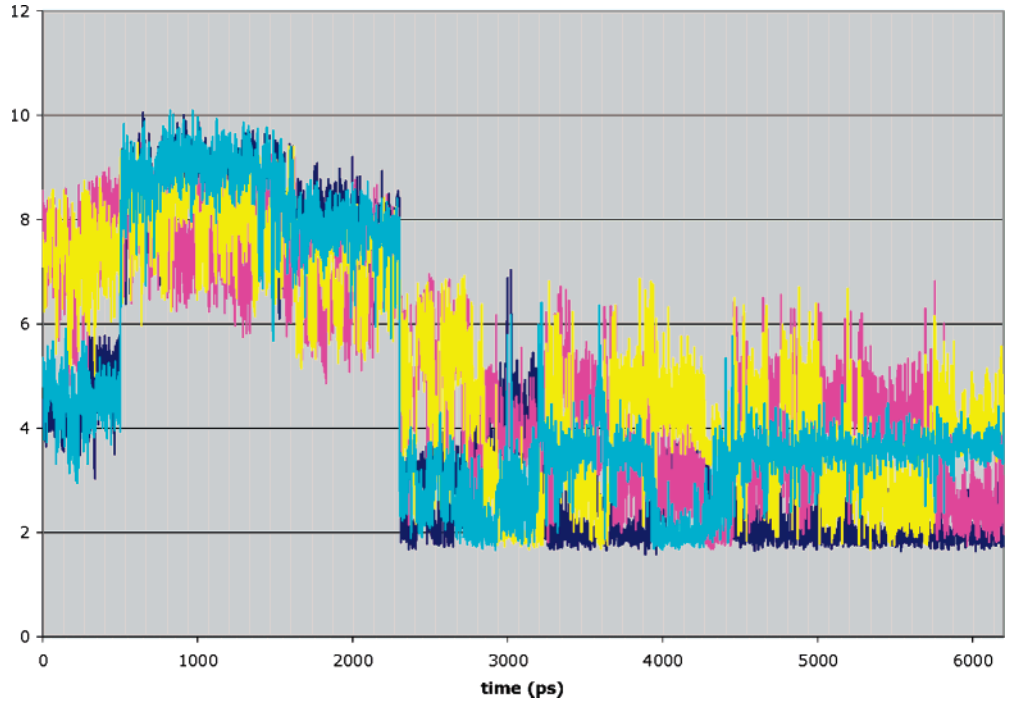

FIGURE 15: Evolution of the distances (in Å) between OD2 at Asp221 and the hydrogen atoms of both NH_2 groups of urea shown in Figure 14. Pink and yellow lines correspond to the hydrogen atoms bound to NU2, whereas the blue and cyan lines represent the distances involving the hydrogen atoms coordinated to NU1.

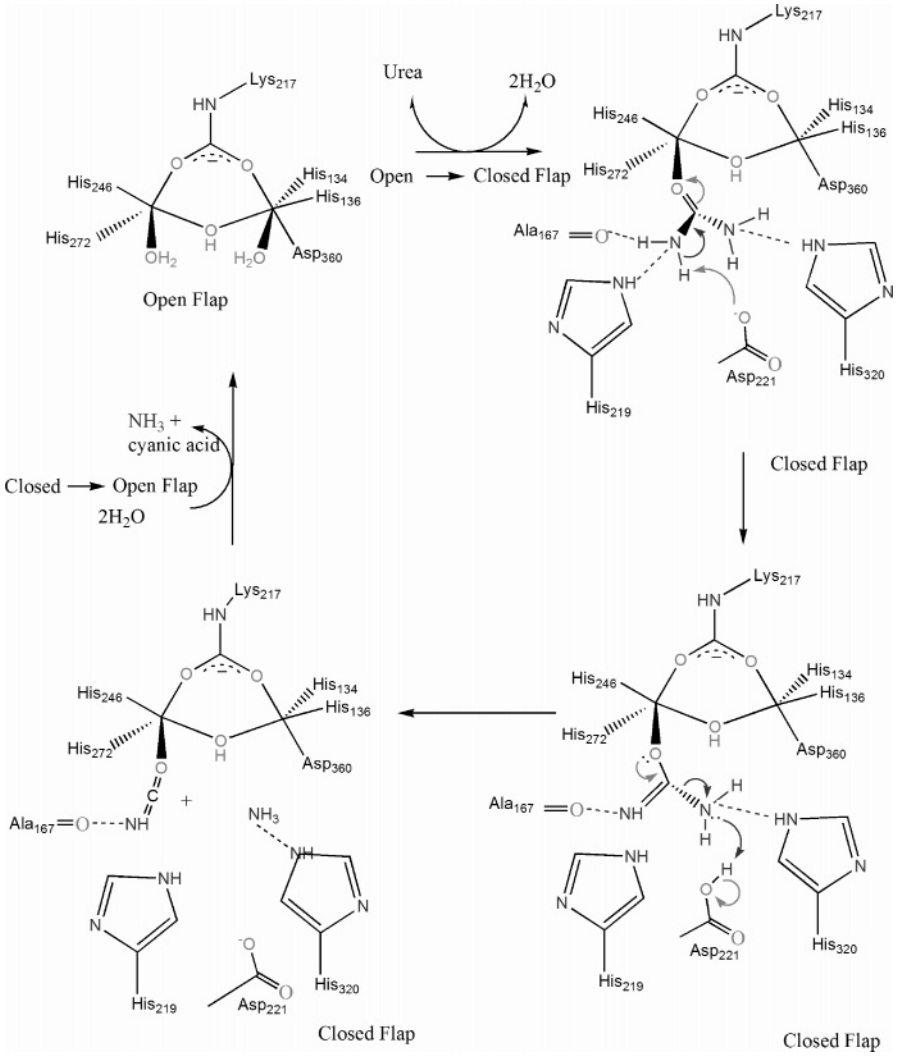

FIGURE 16: Schematic representation of the protein-assisted proton transfer mechanism proposed to occur in the active site of monomer 2.

conserved for the H bound to NU2 (see the blue line in Figure 15), which suggests that NU2 is the proton donor group. Nevertheless, both NH_2 groups of urea alternatively play the role of hydrogen bond donors toward OD2 at Asp221.

From an inspection of Figure 14, it is evident that His219 and His320 can play a role in the mechanism of urea decomposition. While the His residues are oriented in a way that may favor proton transfer to the nitrogen atoms of urea, this role cannot be easily justified given their protonation state and optimum pH of urease (pH = 8). These residues may play more of a role in positioning urea and Asp221 in such a way that allows proton transfer reactions established through long-lived hydrogen bonds (i.e., NU2 at urea−HE2 at His219, HE2 at His219−OD2 at Asp221, ND1 at His320−NU1 at urea. When analyzing the evolution of these hydrogen bond interactions, during the MD simulation (see Figure 2 in the Supporting Information), it is interesting to remark that the protein−urea hydrogen bonds are more fluxional than the hydrogen bonds only involving intraprotein interactions. Although not defining primary interactions in the second monomer, the His residues remain close to urea, ready to assist in the stabilization of the species that result from its decomposition. As an additional role, His320 can assist the release of NH_3 in the way previously described for the first monomer. A schematic representation of our proposed mechanism is shown in Figure 16.

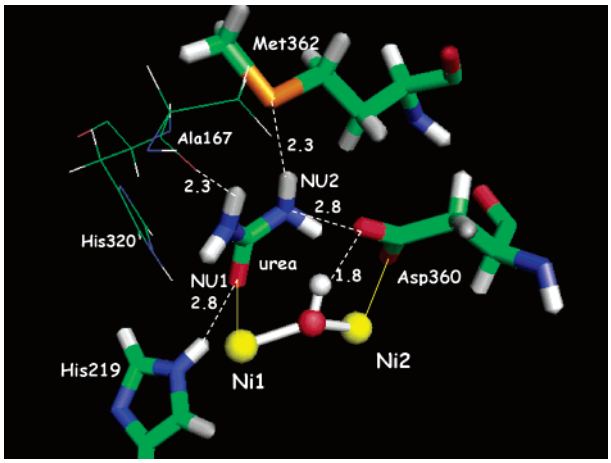

FIGURE 17: Snapshot of UrHisHis showing the most relevant hydrogen bond interactions that are stabilized in the third monomer between the urea ligand and the protein residues. Only the Ni atoms (yellow) and the bridging OH are used to represent the active site. The distances are shown in Å, measured at the end of the 6 ns MD run. A stereographic representation is included in the Supporting Information.

The relevant role proposed here for His219 and His320 in urease-catalyzed urea decomposition is in full agreement

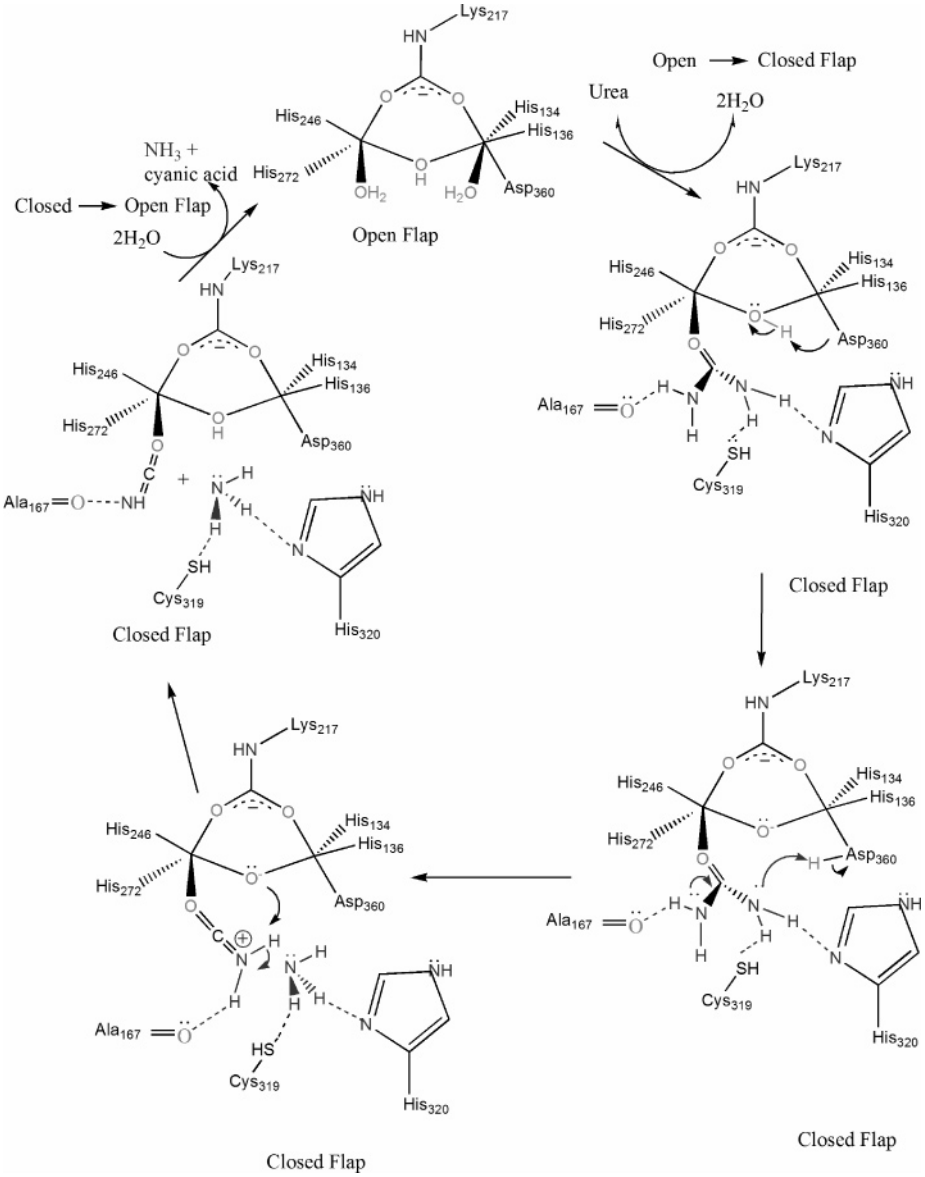

FIGURE 18: Schematic representation of the protein-assisted proton transfer mechanism proposed to occur in the active site of monomer 3.

with the results of mutagenesis studies (*23*−*25*, *27*, *43*−*45*). The former has been proposed to play a role in substrate binding, because the His219Ala mutant has a markedly increased K_M of 1100 mM and a decreased K_{cat} of 60 s^{-1}, yielding a 10^4-fold decrease in k_{cat}/K_M. The His320Ala variant exhibits only moderate changes in K_M but a 10^5-fold reduction in k_{cat} (*62*). The protein-assisted proton transfer mechanism accounts for the participation of both residues in the catalytic mechanism.

The analysis of the third monomer (see Figure 17) indicates that a different mechanism can probably compete with the protein-assisted proton transfer pathway previously described (see Figure 10). In this monomer, the bridging OH establishes a strong hydrogen bond interaction with OD2 at Asp360, which is 2.8 Å away from one of the nitrogen atoms of the urea molecule. In this way, the Asp360 can assist the proton transfer from OH to the NH_2 of urea and the subsequent release of NH_3 (see Figure 18). The time evolution of the key distances indicates that these interactions are stable over the 6 ns MD run [see Figure 19 (gray and cyan)].

This mechanism resembles the one proposed by Benini et al., which was based on the assumption of a bidentate coordination of urea in the urease active site, analogous to the experimentally determined coordination of DAP (*1*). This mechanism also predicts that the release of NH_3 is facilitated by its interaction with His320, which acts as a hydrogen bond acceptor and assists the movement of the leaving NH_3 group when the flexible flap opens. The role of His320 has been extrapolated from an analysis of the hydrogen bond network that is observed in DAP-inhibited urease (PDB code 3UBP). In particular, the hydrogen bonds formed with the free amine of DAP. These include hydrogen bonds between the free DAP NH_2 and O at Ala363, SG at Cys319, and NE at His320 (3.14, 3.25, and 3.8 Å, respectively; distances between heavy atoms) (*1*). Our MD simulations, with urea bound rather than DAP, do not favor the formation of hydrogen bonds between Ala363 and His320 and the free urea NH_2 moiety. We find that Cys319 plays this role and is at a distance of 3.8 Å (SG−NU heavy atom distance) at the end of the MD run. This residue is oriented toward urea, and the hydrogen bond interaction will certainly become stronger after protonation

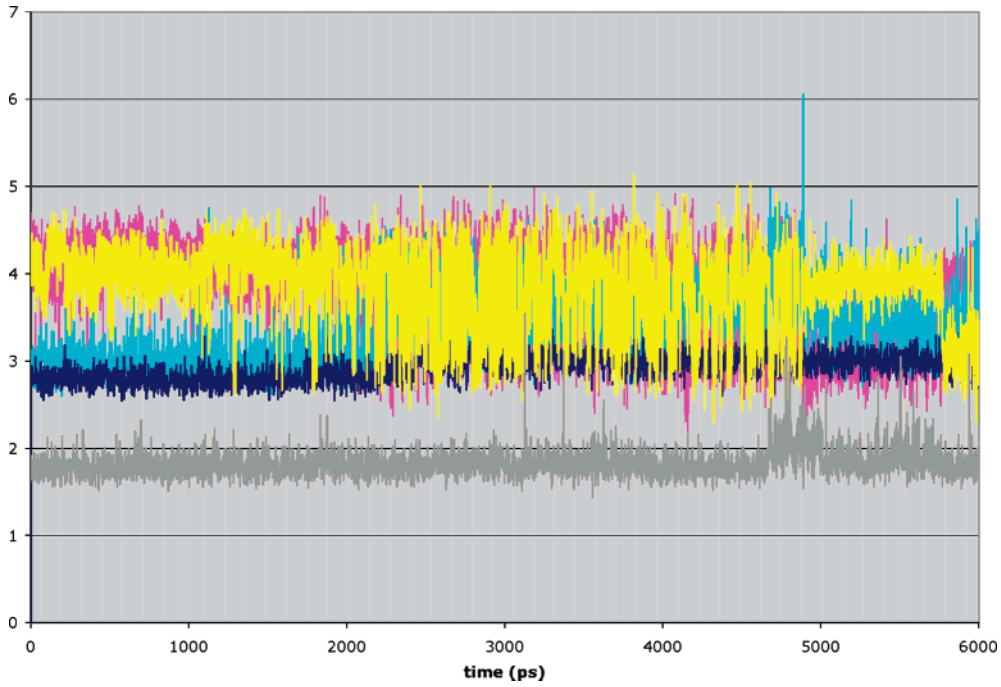

FIGURE 19: Evolution of the distances associated with the interactions shown in Figure 15. Color code: gray, H at OH−OD2 at Asp360; cyan, NU2 at urea−OD2 at Asp360; blue, C at urea−O at OH. Pink and yellow correspond to the interaction of the H atoms at NU2 and O at OH.

of the free NH_2 group of urea. Met362 can also be involved in assisting NH_3 release. This residue, as well as Ala363, changes the orientation of the hydrogen bond acceptor moiety (S and carbonyl, respectively) during flap opening. According to this mechanism, NH_3 release would leave a protonated isocyanic acid coordinated to Ni(1). Deprotonation can easily occur through proton transfer to the bridging hydroxide ion, which can be assisted by Asp360. An additional similarity between the interactions found for the third monomer and those proposed by Benini et al. (*1*) is defined by the role of His219, which acts as a donor toward the Ni(1)-bound oxygen atom (belonging either to DAP or to the urea carbonyl oxygen), polarizing the C−O and C−N bonds.

The mechanism proposed here supports the one described by Benini et al. in predicting the proton transfer from the bridging OH to a NH_2 of urea. However, the mechanism of Benini et al. implies a prior nucleophilic attack of the hydroxide O at WB to the carbonyl carbon of coordinated urea. It results in coordinated carbamate, while the mechanism proposed here yields a coordinated cyanic acid. We favor the latter mechanism, because we have not seen any indications of the bridging O- - -C distance contracting which would indicate the possibility of the formation of a urea carbonyl C—bridging O bond. This distance remains stable with an average value of 2.8 Å (see Figure 19).

From the analysis of the time evolution of the interactions of urea with residues of the active site for the third monomer, we conclude that a reaction mechanism, which is triggered by the same proton transfer (from WB to NH2 at urea) proposed by Benini and co-workers (*1*), can certainly occur. In this case, the assistance of the residues of the mobile flap does not become as relevant as for the protein-assisted proton transfer. In the first two monomers the interactions with residues of the loop become relevant for the determination of the coordination geometry of urea in the active site. However, for the third monomer the coordination geometry is largely determined by the interaction with the bridging OH.

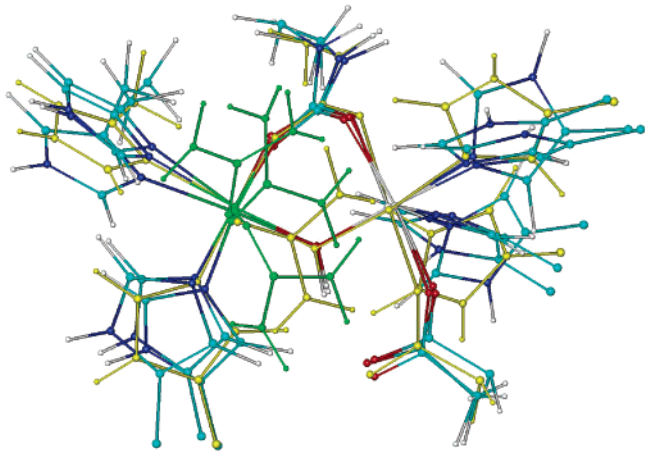

FIGURE 20: Superposition of the active sites of the three monomers after the 6 ns MD run. The structures are superimposed using S3 as template. The urea ligands of the active sites are colored in green, and S3 is shown in yellow.

The stabilization of several different urea/metal cluster interaction patterns in the three active sites is in agreement with the possible existence of different conformations for bidentate urea (see Figure 8). The final structures, compared in Figure 20 using S3 as template, show that the active site is conserved during the 6 ns MD runs, while the urea molecule rotates, as expected, around the Ni−O bond.

(B) Protonated His320, UrHip320. Several experimental observations have suggested that His320 plays a relevant role in urease catalysis (*24*, *62*). In addition to the results of mutagenesis studies, the analysis of urease crystal structures shows significant structural features associated with this residue. In the closed conformation of the mobile flap, His320 is placed at hydrogen-bonding distance from the free NH_2 group of DAP (*1*) or from the same group of a urea-

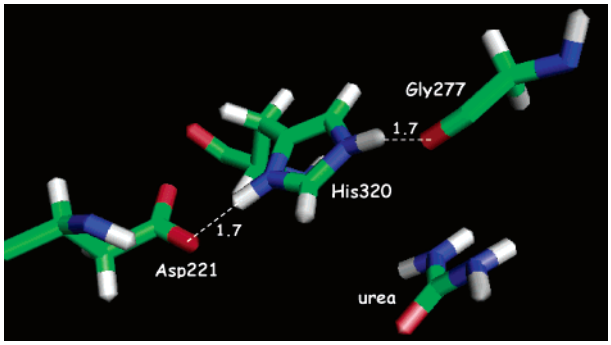

FIGURE 21: Snapshot of UrHip230 showing the hydrogen bond interactions that keep protonated His320 in a preferred orientation. The distances are shown in Å, measured at the end of the 6 ns MD run.

docked molecule (*24*). In light of the structural, biochemical, and computational insights, His320 has been assigned roles as an acidic or basic group. In its role as an acidic group, this residue has been proposed to transfer a proton to an NH_2 of urea and of promoting the release of NH_3 (*63*). This assumption has been justified through the introduction of a reverse protonation hypothesis, according to which 0.3% of the molecules will be in the optimal protonation state for catalysis (*24*).

To account for the possibility that His320 is protonated in urea-complexed urease and to analyze how the protonation state of His320 affects the catalytic mechanism, we have modeled this protonation state and run a 6 ns MD simulation. The result of this analysis is conclusive in showing that the protonation of His320 does not help in the catalytic mechanism. The protonated imidazole nitrogen atoms of this residue form strong hydrogen bonds, acting as donors toward O at Gly277 and OD2 at Asp221. These interactions remain stable over the entire 6 ns MD simulation (see Figure 3 in the Supporting Information), holding His320 in an orientation that can be described as parallel to the bound urea molecule and, thereby, preventing it from assisting the catalytic reaction mechanism. This behavior is exemplified in Figure 21 for the case of the first monomer only (the second and third monomers give analogous results).

(C) Protonated His219, UrHip219. The protonation state of His219 is also important because this residue is positioned in a way that favors hydrogen bonding to either the Ni-bound oxygen of DAP (*1*) or the carbonyl oxygen of Ni-coordinated urea (*24*). However, the results of our MD simulations show that neutral His219 is not electrophilic enough to retain the hydrogen bond interaction initially formed with the carbonyl oxygen (see Figure 9). Considering the possibility that His219 takes up a proton, we have carried out a MD simulation where His219 is protonated to see if the lifetime of the hydrogen bond interactions between His219 and urea is increased. A snapshot obtained after 6 ns is shown in Figure 22 for one of the three different monomers. For all monomers it is evident that the increase of the electrophilicity of His219 through protonation stabilizes the N−H- - -O H-bonds, which are characterized by average HE2 at His219−O at urea distances of 2.2, 2.5, and 2.6 Å for the first, second, and third monomers, respectively (see Figure 4 in the Supporting Information). This interaction, together with the coordination of urea to the positive Ni center, activates the molecule by polarizing the C−O and C−NH_2 bonds. In addition, it helps to position the urea ligand in a way that favors its interaction with the bridging OH, assisted by the Asp360 residue. A hydrogen bond interaction with OD1 at Asp360 distorts the urea ligand from planarity in a way that has already been found in intermediate steps of the decomposition of urea in acid media. The energy cost associated with this distortion can certainly be overcome by the hydrogen bond interactions shown in Figure 22. As a result, the mechanism previously described for the third monomer of the UrHisHis system becomes favored in this case for the three monomers. In this mechanism, NH_3 is formed after proton transfer from the bridging OH, assisted by Asp360. Cys319 guides its release during flap opening, together with Ala363 and Met362, whose carbonyl and S groups are rotated away in the open conformation of the loop. The interaction pattern shown in Figure 22 further supports proton transfer from NU1 to the bridging Ni oxygen atom as the step that follows NH_3 release.

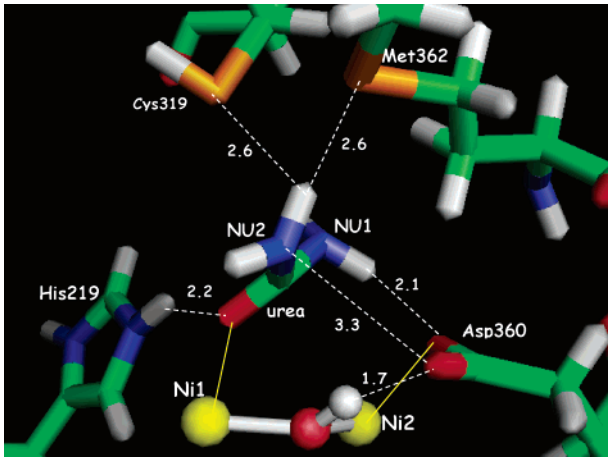

FIGURE 22: Representative snapshot of UrHip219 showing the most relevant hydrogen bond interactions that are stabilized in the third monomer between the urea ligand and protein residues. The Ni atoms (yellow) and the Asp360 residue are used to represent the active site. The distances are shown in Å, measured at the end of the 6 ns MD run.

From the comparison of the behavior found for this system and for UrHisHis, we conclude that the mechanism that involves proton transfer from the bridging OH to the amide nitrogen of urea is favored by polarization of the coordinated urea by a hydrogen bond from His219. A similar mechanism has been proposed by Benini et al. on the basis of the analysis of the hydrogen bond network present in DAP-inhibited urease. The oxygen atom of DAP involved in hydrogen bond coordination with His219 is negatively charged and, hence, more nucleophilic than the carbonyl oxygen atom of coordinated urea, which might explain our observation that neutral His219 does not form strong hydrogen bonds with urea. For the urea molecule to form a stable hydrogen bond interaction, His219 had to be protonated. Nevertheless, the neutral form is the most probable one at the optimum pH of the enzyme, and this mechanism has to compete with the protein-assisted proton transfer one.

CONCLUSIONS

MD simulations of the metalloenzyme urease, complexed with its substrate urea, have provided new insights into the mechanism of urea decomposition. In agreement with

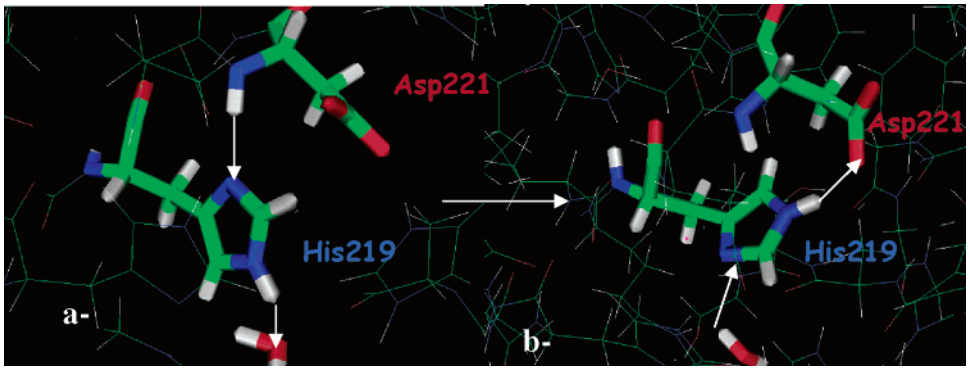

FIGURE 23: H-bond interactions comprising the His219 residue in the first (a) and last (b) snapshots of the 6 ns MD trajectory.

mutagenesis experiments, the simulations emphasize the critical role played by residues of the mobile flap, namely, His320, Cys319, Ala363, and His219 (*23*, *24*, *43*, *44*), as well as the relevance of the bridging hydroxyl (*1*, *19*−*22*). Moreover, several different mechanisms have been proposed for the urease-catalyzed reaction on the basis of biochemical studies, and several questions remain open, which are mainly related to the coordination mode of urea to the Ni metallocenter and to the potential protonation states of His219 and His320 (*1*, *19*−*22*). To provide significant answers to these open questions, we have analyzed three different systems, associated with different protonation states of His320 and His219.

The time-averaged structures observed in the three monomers suggest that urease could follow two different competitive mechanisms. The protein-assisted proton transfer mechanism largely relies on the assistance of protein residues, centering on Asp221 as relevant for catalysis (see Figures 10 and 14). The role of this residue has been discussed in the literature (*44*), and it has been assumed to stabilize the substrate (or inhibitor) bound to Ni(1). The second proposed mechanism, which can be described as "Asp-mediated proton transfer" is mainly restricted to the residues of the active site and involves the transfer of a proton from the bridging OH to an NH_2 of urea, assisted by the Asp residue of the active site (see Figure 17). This proton transfer leaves a very reactive nucleophilic group (di-Ni-coordinated oxygen) capable of attacking the carbonyl carbon atom of urea to form the tetrahedral intermediate characteristic of the hydrolytic pathway. In this way, from the analysis of the third monomer, we conclude that elimination and hydrolytic mechanisms can compete in the urease active site, leading to isocyanic acid or carbamic acid, respectively, coordinated to Ni(1) (see Figures 13, 16, and 18). The hydrolysis of the products will ultimately result in CO_2 and NH_3.

From the comparative analysis of the time evolution of the three systems associated with different protonation states of His320 and His219 we have derived the following conclusions: (i) The protein-assisted proton transfer and the Asp-mediated proton transfer mechanisms compete for the decomposition of urea when both His residues are in their neutral protonation state. (ii) The protonated form of His320 does not favor the active participation of this residue in the catalytic mechanism. (iii) The protonated form of His219 favors the mechanism that proceeds through proton transfer from the bridging OH to the free NH_2 of urea, mediated by Asp360.

On the basis of the known optimum pH for urease catalytic activity (pH = 8), we feel it unlikely that His219 is protonated. However, the last major conclusion leads us to reevaluate the role of His219, which is known to strongly contribute to substrate binding (*1*). It has been assumed, for more that a decade, that His219 is in its neutral NE-protonated form: the NE atom donates a hydrogen bond to the water molecule bound to Ni(1), while it accepts a hydrogen bond at the ND nitrogen from the main chain nitrogen of Asp221 (*1*, *24*, *43*, *44*, *62*). However, MD simulations of the native enzyme (*64*) indicate that the hydrogen bond network surrounding His219 fluctuates as shown in Figure 23. In this figure, the first and last snapshots of the 6 ns trajectory are shown. In the latter, His219 has rotated around the CG−CB bond, establishing a hydrogen bond from HE to Asp221 (NE−HE- - -OD2 at Asp221), and accepts a hydrogen bond from a water molecule of the active site to ND. This pattern is repeated in the three monomers of the trimeric enzyme and suggests that the actual form of His219 is as the ND-protonated neutral form. However, this possibility is at variance with the proposed coordination of His219 with an oxygen of DAP in the DAP-inhibited urease structure (PDB code 3UBP). However, the position of the OH in $PO(OH)(NH_2)$ has not been uniquely determined, nor can the precise location of the nitrogen atoms be uniquely identified by the X-ray experiment (*1*, *21*). Thus, the possibility that the hydrogen bond pattern is as we observe is not disallowed by the available experimental information. Moreover, in the case of bound urea it might be favored over that suggested for the DAP-inhibited enzyme.

The resolution of the X-ray determinations for the urease enzyme and its variants (∼2.0 Å) (*1*, *20*−*23*, *25*, *43*−*45*, *62*) allows us to consider several structures that are compatible with the reported diffraction pattern. We are analyzing this issue in detail at different levels of theory, as we have found the role of His219 to strongly determine the mechanism of the catalyzed urea decomposition.

Examination of the catalytic mechanisms of enzymes using computational tools is difficult, and the present MD simulations demonstrate this point further. Indeed, depending on the specific active site studied and at what point in the MD simulation, we found that several pathways were possible based on the hydrogen-bonding network present. Moreover, we have found that both hydrolytic and elimination mechanisms are possible using active site cluster models which even further complicate the overall picture. Competitive mechanisms are frequently found for enzymatic reactions,

as a consequence of the complicated energy landscape associated with these biological processes (*65*). Theoretical approaches have the potential to link structural and biochemical observations at the molecular level, but it is clear that combinations of QM studies on cluster models coupled with QM/MM, long MD simulations, and biochemical data will, at least in the case of urease, be necessary to provide definitive insights into the catalytic mechanism of this enzyme.

SUPPORTING INFORMATION AVAILABLE

Bond and angle parameters involving the di-Ni urease metallocenter, RESP atomic charges for the Ni atoms and Ni ligands, plots showing the evolution of relevant distances during the MD runs, and stereographic representations of the active sites of the three urease monomers. This material is available free of charge via the Internet at http://pubs.acs.org.

REFERENCES

1. Benini, S., Rypniewski, W. R., Wilson, K. S., Miletti, S., Ciurli, S., and Mangani, S. (1999) *Struct. Folding Des. 7*, 205−216.
2. Hoops, S. C., Anderson, K. W., and Merz, K. M. J. (1991) *J. Am. Chem. Soc. 113*, 8262−8270.
3. Garcia-Viloca, M., Gao, J., Karplus, M., and Truhlar, D. (2004) *Science 303*, 186−195.
4. Kuchar, J., and Hausinger, R. P. (2004) *Chem. Rev. 104*, 509−526.
5. Noodleman, L., Lovell, T., Han, W., Li, X., and Himo, F. (2004) *Chem. Rev. 104*, 459−508.
6. Tshuva, E., and Lippard, S. J. (2004) *Chem. Rev. 104*, 987−1012.
7. Schnell, P., Dyson, H. J., and Wright, P. E. (2004) *Annu. Rev. Biophys. Biomol. Struct. 33*, 119−140.
8. Solomon, E. I., Szilagyi, R. K., DeBeer, G. S., and Basumallick, L. (2004) *Chem. Rev. 104*, 419−458.
9. Weston, J. (2005) *Chem. Rev. 105*, 2151−2174.
10. Zhang, X., and Houk, K. N. (2005) *Acc. Chem. Res. 38*, 379−385.
11. Warshel, A. (1998) *J. Biol. Chem. 273*, 27035−27038.
12. Dewar, M. J., and Storch, D. M. (1985) *Proc. Natl. Acad. Sci. U.S.A. 82*, 2225−2229.
13. Bruice, T. C. (2002) *Acc. Chem. Res. 35*, 139−148.
14. Westheimer, F. H. (1962) *Adv. Enzymol. 24*, 441−482.
15. Kraut, D. A., Carroll, K. S., and Herschlang, D. (2003) *Annu. Rev. Biochem. 72*, 517−571.
16. Warshel, A., Strajbl, M., Villa, J., and Florian, J. (2000) *Biochemistry 29*, 14728−14738.
17. Estiu, G. L., and Merz, K. M. J. (2004) *J. Am. Chem. Soc. 126*, 6932−6944.
18. Callahan, B. P., Yuan, Y., and Wolfenden, R. (2005) *J. Am. Chem. Soc. 127*, 10828−10829.
19. Benini, S., Ciurli, S., Rypniewski, W. R., Wilson, K. S., and Mangani, S. (1998) *Acta Crystallogr. D 54*, 409−412.
20. Benini, S., Rypniewski, W. R., Wilson, K. S., Ciurli, S., and Mangani, S. (1998) *J. Biol. Inorg. Chem. 3*, 268−263.
21. Benini, S., Rypniewski, W. R., Wilson, K. S., Ciurli, S., and Mangani, S. (2001) *J. Biol. Inorg. Chem. 6*, 778−790.
22. Benini, S., Rypniewski, W. R., Wilson, K. S., Mangani, S., and Ciurli, S. (2004) *J. Am. Chem. Soc. 126*, 3714−3715.
23. Jabri, E., and Karplus, A. (1996) *Biochemistry 35*, 10616−10626.
24. Karplus, P. A., Pearson, M. A., and Hausinger, R. P. (1997) *Acc. Chem. Res. 30*, 330−337.
25. Jabri, E., Carr, M. B., Hausinger, R. P., and Karplus, P. A. (1995) *Science 268*, 998−1004.
26. Todd, M. J., and Hausinger, R. P. (2000) *Biochemistry 39*, 5389−5396.
27. Todd, M. J., and Hausinger, R. P. (1991) *J. Biol. Chem. 266*, 24327−24331.
28. Wang, J., and Tarr, D. (1955) *J. Am. Chem. Soc. 77*, 6205−6206.
29. Blakeley, R. L., Hinds, J. A., Kunze, H., Webb, E. C., and Zerner, B. (1969) *Biochemistry 8*, 1991−2000.
30. Mack, E., and Villars, D. E. (1923) *J. Am. Chem. Soc. 45*, 505−510.
31. Barrios, A. M., and Lippard, S. J. (1999) *J. Am. Chem. Soc. 121*, 11751−11757.
32. Barrios, A. M., and Lippard, S. J. (2000) *J. Am. Chem. Soc. 122*, 9172−9177.
33. Barrios, A. M., and Lippard, S. J. (2001) *Inorg. Chem. 40*, 1250−1255.
34. Estiu, G. L., and Merz, K. M. J. (2004) *J. Am. Chem. Soc.* (in press).
35. Dunn, B. E., and Grutter, M. G. (2001) *Nat. Struct. Biol. 8*, 480−482.
36. Dunn, B. E., Cohen, H., and Blaser, M. J. (1997) *Clin. Microbiol. Rev. 10*, 720−741.
37. Covacci, A., Telford, J. L., Del Giudice, G., Parsonnet, J., and Rappuoli, R. (1999) *Science 284*, 1328−1333.
38. Lockamy, V. L., Huang, J., Shields, H., Ballas, S. K., King, S. B., and Kim-Shapiro (2003) *Biochim. Biophys. Acta 1622*, 109−116.
39. Holz, R. C. (2002) *Coord. Chem. Rev. 232*, 5−26.
40. Porter, T., Li, Y., and Raushel, F. (2004) *Biochemistry 43*, 16285−16292.
41. Lippard, S. J. (1995) *Science 268*, 996−997.
42. Musiani, F., Arnolfi, E., Casadio, R., and Ciurli, S. (2001) *J. Biol. Inorg. Chem. 6*, 300−314.
43. Pearson, M. A., Michel, L. O., Hausinger, R. P., and Karplus, P. A. (1997) *Biochemistry 36*, 8164−8172.
44. Pearson, M. A., Prk, I.-S., Schaller, R. A., Michel, L. O., Karplus, P. A., and Hausinger, R. P. (2000) *Biochemistry 39*, 8575−8584.
45. Pearson, M. A., Schaller, R. A., Michel, L. O., Karplus, P. A., and Hausinger, R. P. (1998) *Biochemistry 37*, 6214−6220.
46. Suarez, D., Diaz, N., and Merz, K. M. J. (2003) *J. Am. Chem. Soc. 125*, 15234−15247.
47. Zerner, B. (1991) *Biorg. Chem. 19*, 116−131.
48. Kuhler, T. C., Fryklund, J., Bergman, N., Weilitz, J., Lee, A., and Larsson, H. (1995) *J. Med. Chem. 38*, 4906−4916.
49. Case, D. A., Darden, T., Cheatham, C. L., III, Simmerling, C. L., Wang, J., Duke, R. E., Luo, R., Merz, K. M., Wang, B., Pearlman, D. A., Crowley, M., Brozell, S., Tsui, V., Gohlke, H., Mongan, J., Hornak, V., Cui, G., Beroza, P., Schafmeister, C., Caldwell, J. W., Ross, W. S., and Kollman, P. A. (2004) Amber8.
50. Van Gusteren, W. F., and Berendsen, H. J. C. (1977) *Mol. Phys. 34*, 1311.
51. Allen, M. P., and Tildesley, D. J. (1987) *Computer Simulation of Liquids*, Claredon Press, Oxford.
52. Essman, V., Perera, L., Berkowitz, M. L., Darden, T., Lee, H., and Pedersen, L. G. (1995) *J. Chem. Phys. 103*, 3668−3679.
53. Fox, T., and Kollman, P. A. (1998) *J. Phys. Chem. B 102*, 8070−8079.
54. Suarez, D., and Merz, K. M. J. (2001) *J. Am. Chem. Soc. 123*, 3759−3770.
55. Becke, A. D., and Yarkony, D. R. (1995) in *Modern Electronic Structure Theory*, Part II, World Scientific, Singapore.
56. Jaguar (1998) Scrodinger Inc., Portland, OR.
57. Hay, P. J., and Wadt, W. R. (1985) *J. Chem. Phys. 82*, 299−310.
58. Hehre, W. J., Radom, L., Schleyer, P. v. R., and Pople, J. A. (1986) *Ab Initio Molecular Orbital Theory*, John Wiley & Sons, New York.
59. Dunietz, B. D., Beachy, M. D., Cao, Y., Whittington, D. A., Lippard, S. J., and Friesner, R. A. (2000) *J. Am. Chem. Soc. 122*, 2828−2839.
60. Bayly, C. A., Cieplak, P., Cornell, W., and Kollman, P. A. (1993) *J. Phys. Chem. 97*, 10269−10280.
61. Diaz, N., Sordo, T. L., Merz, K. M. J., and Suarez, D. (2003) *J. Am. Chem. Soc. 125*, 672−684.
62. Park, I., and Hausinger, R. P. (1993) *Protein Sci. 2*, 1034−1041.
63. Karplus, A. (2002) *Acc. Chem. Res. 35*, 321−323.
64. Estiu, G. L., and Merz, K. M., Jr., unpublished results.
65. Basner, J. E., and Schwartz, S. D. (2005) *J. Am. Chem. Soc.* (in press).

BI052020P